Nuclear Instruments and Methods in Physics Research B 574 (2026) 166081

Contents lists available at ScienceDirect

Nuclear Inst. and Methods in Physics Research, B

journal homepage: www.elsevier.com/locate/nimb

Full Length Article

Superfocusing of channelled protons – anharmonic oscillation model☆

Žiga Šmit [a,b,*], Esther Punzon-Quijorna [b], Sabina Markelj [b]

[a] Faculty of Mathematics and Physics, University of Ljubljana, Ljubljana, Slovenia
[b] Jožef Stefan Institute, Ljubljana, Slovenia

A B S T R A C T

Focusing of channelled ions just below the crystal surface, known as superfocusing, was treated analytically as a combination of straight movement along the channel axis and perpendicular oscillations of an anharmonic oscillator. The anharmonic term in the channel potential is responsible for dispersion of the trajectories. It was shown that the anharmonic term vanishes for a specific oscillation plane along the <1 0 0> channel, which would in principle allow a very sharp focusing point. However, the focusing pattern is blurred due to the multiple scattering by electrons. This effect, which was estimated from the projectile energy loss calculated for axially dependent electron density, can completely obscure the focusing effect from the second focusing point onwards.

1. Introduction

Numerical simulations have shown that a parallel beam of channelled particles is periodically densified when travelling along the crystal channel [1–6]. Sharp border of the densified region gave name to the rainbow effect [1–4], though more recent investigations concentrate on the focusing effect of the channeled particles within the channel cross section, which lead to another name, superfocusing [5,6]. As a tempting application, by slightly tilting the impact angle, the focused beam can hit an impurity atom in the middle of the channel at different impact parameters [6]. Experimental evidence of the effect involves detection of characteristic angular distribution of channeled particles leaving a thin crystal, using a position sensitive or scintillation detector [7–9]. The measured distribution of scattered particles is generally well reproduced by Monte Carlo simulations, though the detection of true focusing point and simulation of its realistic dimensions is still not very clear.

The purpose of the present calculations is to provide a transparent model of superfocusing process, with an aim to study the sharpness of the focusing points.

Focusing effect of the channeled particles can be explained by simple physical principles. Channeled particles move in transverse direction in a combined potential of atomic rows, which is harmonic in its first approximation. When entering the crystal, the impact particles travelling parallel with the channel axis can be regarded as being at amplitude displacement of their transverse motion. They start moving towards the equilibrium position at the channel axis at the same time, and as the oscillation time of the harmonic oscillations does not depend on amplitude, all particles reach the channel axis simultaneously. Since particles at the same time travel along the channel axis, focusing appears at the same distance from the crystal surface. With further oscillation, the focusing points appear at periodic distances along the channel axis.

This ideal image is spoiled by several effects. (1) The transverse potential deviates from the harmonic approximation, which causes dispersion of the focusing distances as a function of the distance from the axis channel. (2) Electron density in the channel also varies, so the particles with greater amplitudes lose more energy than the particles near the channel axis. This causes particles with greater amplitudes to experience greater energy loss and have shorter focusing lengths, contributing to further dispersion of focal lengths. (3) Particle collisions with electrons and thermal vibrations of the atoms statistically smear the velocity distribution of the channeled particles and more importantly, smear the angles of particle trajectories. Experimental uncertainties, such as beam energy spread and angular distribution, may further screen the focusing effect.

In the present study, we decided to model particle movement analytically, expanding the channel potential until the first anharmonic term. This will allow us to calculate the distribution of focal lengths in the same way as the caustic curve of spherical mirror. The planar distribution along the particle trajectory will be calculated at different distances along the channel axis until the first focusing point and beyond until defocusing. We will adopt the continuous model of the atomic row potential, studying different approximations of the atomic potential. The calculation will choose as an example 3 MeV protons, which are generally obtainable from small electrostatic accelerators, including the one at Jožef Stefan Institute. Protons were chosen as the starting case and as projectiles that can induce nuclear reactions or X-ray emission in

☆ This article is part of a special issue entitled: '2025 IBA ? PIXE' published in Nuclear Inst. and Methods in Physics Research, B.

* Corresponding author at: Faculty of Mathematics and Physics, University of Ljubljana, Ljubljana, Slovenia.
E-mail address: ziga.smit@fmf.uni-lj.si (Ž. Šmit).

https://doi.org/10.1016/j.nimb.2026.166081
Received 13 December 2025; Received in revised form 2 March 2026; Accepted 6 March 2026
Available online 14 March 2026

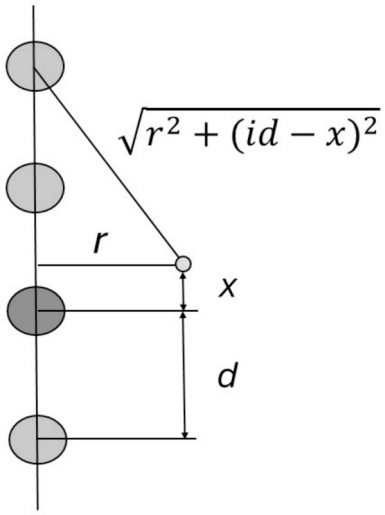

Fig. 1. Geometry for calculation of the mean potential of a row of atoms, spaced by the distance *d*. The channeled particle moves parallel with the row at a distance *r* and is currently a distance *x* along its path. The index *i* sums the atoms in the row.

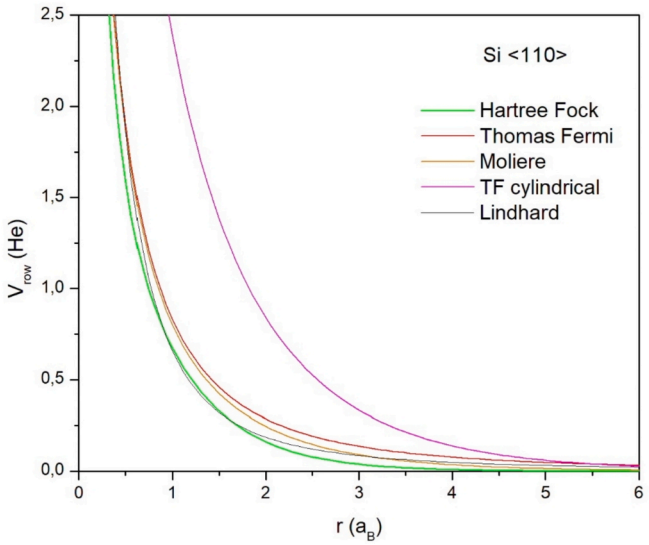

Fig. 2. Mean row potential calculated within Hartree-Fock, Thomas-Fermi, Molière, Lindhard and cylindrical TF model (atomic units).

impurity atoms located inside the channels. Calculation will be done for a proton beam shot perpendicularly at silicon crystals in two significant orientations.

2. The atomic row potential

According to the interpretation of Lindhard [10], the channel particles move in the potential of individual atomic rows. As a collision with an individual atom only minutely changes the particle direction, an average value of the atomic potential can be calculated. Here we followed the same principle for an average potential (Fig. 1):

$$V_r(r) = \frac{2}{d}\int_0^{\frac{d}{2}} \sum_i V\left(\sqrt{r^2 + (id - x)^2}\right) dx \tag{1}$$

with d the interatomic distance and r the distance of the channeling particle from the string. Summation i included the nearest atoms. With respect to original expression [10], we use a realistic upper integration limit (instead of infinity in [10]); this choice is not so important, as atomic potential rapidly approaches zero far from the atom. V is the potential of an individual atom. Here we considered the following approximations:

2.1. Hartree Fock atom

The electronic wave functions of silicon atom were calculated from the HF86 program [11]. Electron density of the whole atom was calculated as a sum of electron densities for individual shells $\rho = \sum_i |\psi_i|^2$, from which the potential of the electron cloud was obtained as

$$\mathrm{V}(r) = \frac{1}{r}\int_\infty^r \rho(r')dr' - \int_\infty^r \rho(r')\, d(\log r') \tag{2}$$

The integration procedure was simple trapezoidal executed on the given HF86 result table; its accuracy was 0.0003, which we checked for the normalization condition $\int \rho(r)dr = Z$.

2.2. Thomas-Fermi approximation

We tried to directly solve the Thomas Fermi differential equation as given in textbooks of quantum mechanics [12]. For this procedure it is necessary to know in addition the starting value of the first derivative of atomic screening function at $r = 0$. Due to error propagation in our code, it was found empirically that for obtaining a stable solution (with results matching those in [12]) it was necessary to assume a value slightly smaller (by 1.8e-6) than its accurate value [13].

2.3. Molière approximation of Thomas-Fermi equation

An analytic approximation to the Thomas-Fermi screening function is given as a sum of three exponential functions [14]. For the proton charge being one, the length unit in this expression was simply assumed as 0.8853 $a_B/Z^{1/3}$.

2.4. Linhard potential

Integrating Eq. (1) with the upper integration limit set to infinity and assuming Thomas-Fermi approximation, Lindhard [10] developed the potential

$$V_r(r) = \frac{Z}{d}\log\left[\left(\frac{Ca}{r}\right)^2 + 1\right] \tag{3}$$

with $C^2 \approx 3$ and a given by 0.8853 $a_B/Z^{1/3}$.

2.5. Two-dimensional Thomas/Fermi model

It seemed challenging to develop a screened-potential model for a longitudinal charged string of linear charge distribution Ze_0/d and encircled by a diffuse negative charge composed of electrons with the same linear density. A Thomas-Fermi model in cylindrical geometry has already been studied [15], but the details do not comply with our case.

In an area dS, the number of electrons with momentum smaller than p is equal to $p^2/2\pi$ according to the available phase space, while the volume density of the particles is $n = p^2/2\pi d$ (we use atomic units, Bohr radius for length and Hartree for energy, respectively). As in the three-dimensional case we write for the kinetic energy $p^2/2 = \varphi - \varphi_0$ and set the potential φ_0 far from the string to zero. The electron density is then expressed as $n = \varphi/\pi d$. From the Poisson equation $\Delta\varphi = -e_0 n/\varepsilon_0$, we find in cylindrical coordinates

$$r^2\frac{d^2\varphi}{dr^2} + r\frac{d\varphi}{dr} - \frac{4r^2}{d}\varphi = 0 \tag{4}$$

The solutions of this equation are modified Bessel function of zero order.

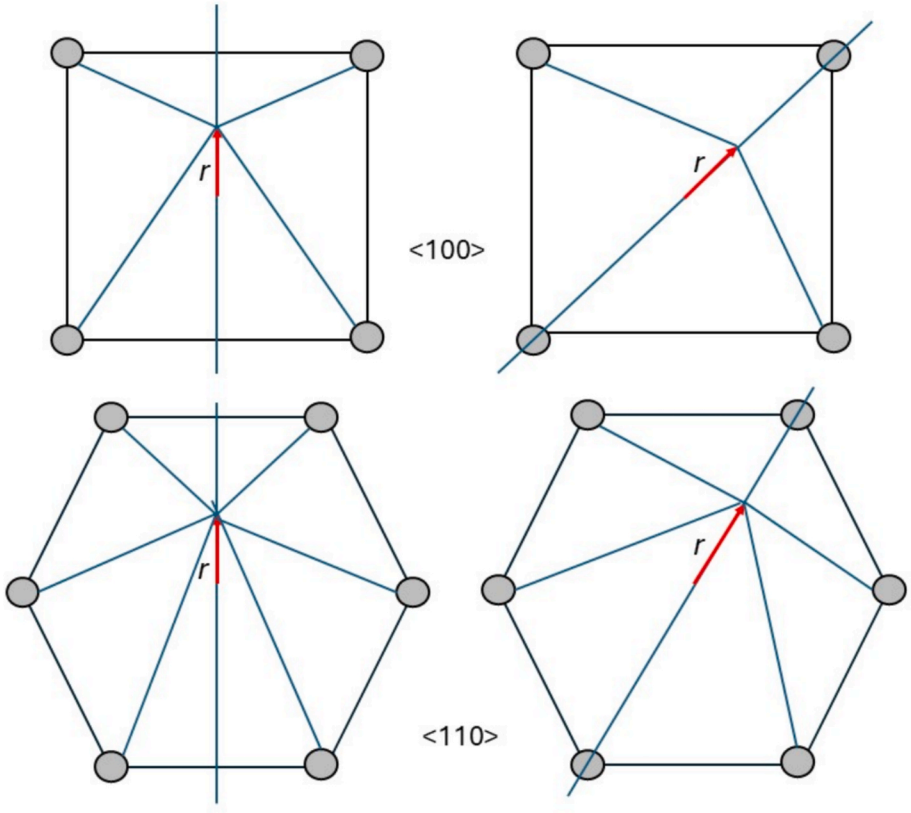

Fig. 3. <1 0 0> and <1 1 0> channels in silicon. The red arrows point to the selected oscillation planes a, b and expansion of the potential in this direction.

As the potential tends to zero for infinite r, the potential is proportional to $K_0(2r/\sqrt{d})$. The proportional constant is obtained by the condition that Z electrons are contained in one unit cell: $Z/d = \int n\ 2\pi r\ dr$. The potential of the charged string dressed in an opposite charge of electrons is then

$$\varphi(r) = \frac{2Z}{d} K_0\left(\frac{2r}{\sqrt{d}}\right) \tag{5}$$

One can verify that in the limit $r \to 0$, the potential varies logarithmically with r.

The atomic row potential for all five approximations is shown for silicon in <1 1 0> direction (Fig. 2) where the interatomic distance is 0.3840 nm (7.2571 in atomic units). It is evident that the two-dimensional Thomas-Fermi model overestimates the other four models. By numerical variation of parameters, it was possible to check that these differences diminish with the reduced interatomic distance d. We can interpret this finding that for the actual interatomic distance, the atoms retain their individual character and do not merge into a single string. The differences between the remaining approaches are small. For the ongoing calculation we decided to use the row potential as calculated from Hartree Fock electron densities, as this method is closest to first order principles; its values are slightly smaller than the others.

3. The channel potential

The potential in the inner part of the channel was calculated by summing row potentials of individual atomic rows that border the channel. For Si <1 1 0> they were six, for Si <1 0 0> four. As we wanted to see the effect of potential anharmonicity, we first chose two characteristic oscillation directions in each channel, which coincided with one of the mirror planes (Fig. 3). The potential was optimally fitted to the expression

Table 1
Coefficients k and k_1 for the channel potential in silicon in <1 0 0> and <1 1 0> directions, for two oscillations planes as marked in Fig. 3.

Oscillation direction	k (Hartree/a_B^2)	k_1 (Hartree/a_B^4)
<1 0 0> a	0.15279	0.150108
<1 0 0> b	−5.5749e-2	9.6056e-2
<1 1 0> a	2.5173e-2	4.1652e-3
<1 1 0> b	2.3333e-2	7.6577e-3

$$V_{ch}(r) = V_0 + \frac{1}{2}kr^2 + \frac{1}{4}k_1 r^4 \tag{6}$$

choosing r^2 as an independent variable. The coefficients k and k_1 determine the oscillation frequency and departure from the harmonic model (Table 1).

It is significant that the coefficients k differ very little for two oscillation planes in <1 0 0> direction (by 1.8%), while the coefficient k_1 changes sign. This means that there are oscillation planes within the <1 0 0> channel where focusing may be perfect, without dispersion. The situation is different for the <1 1 0> channel, as there is a larger difference between the coefficients k (by 7.9%) and the coefficient k_1 does not change sign, implying higher dispersion.

4. The anharmonic oscillations

The presence of anharmonic term in the channel potential implies the following oscillation equation:

$$m\ddot{y} + ky + k_1 y^3 = 0 \tag{7}$$

Accurate solutions of Eq. (7) can only be found numerically, however for small perturbation of the anharmonic term we also look for an approximate analytical solution. We expect that the transverse

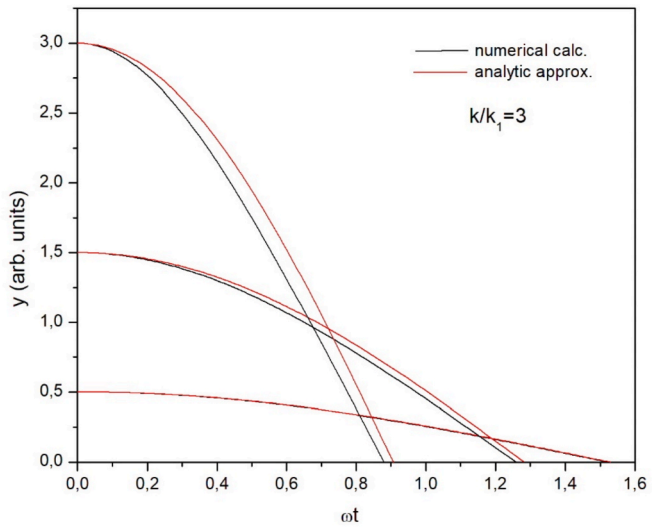

Fig. 4. Oscillation movement within the first quarter of the oscillation time, according to rigorous calculation and approximation of eq. (6).

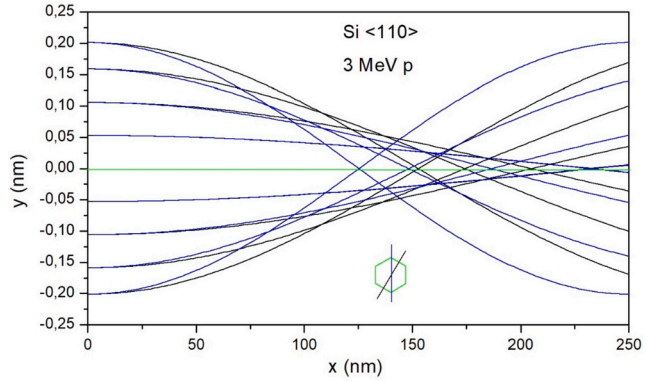

Fig. 5. Proton trajectories in <1 1 0> direction, for two significant oscillation planes.

movement in the channel is still approximately harmonic, but with a different oscillation frequency: $y = A \sin \omega t$. According to the method of Galerkin [16], the approximate solution is orthogonal to the operator in Eq. (7), which is achieved by integration within the half oscillation time. We get

$$\omega = \omega_0 \sqrt{1 + \frac{2}{3}\frac{k_1}{k}A^2} \tag{8}$$

where obviously $\omega_0 = \sqrt{\frac{k}{m}}$. The oscillation frequency of the anharmonic oscillator is amplitude dependent, which would cause dispersion of focusing points in the channel. The accuracy of eq. (8) was checked numerically for different values of the coefficient k_1. Above the ratio $k/k_1 = 3$, the oscillation time was estimated to be better than 3.5% (Fig. 4).

5. Ray tracing

In mirror planes, as shown in Fig. 3, oscillation is planar and can be shown in a simple x-y plot. Moving along the channel was calculated as a retarded linear motion. For the stopping force we first considered a first order approximation, multiplying the stopping power for an amorphous target by the ratio of local and mean electron density: $S_{ch}(E, y) = S(E)\,\rho(y)/\rho_0$. In later development of calculations, we switched to the theoretical stopping power [17] for excitation of electron gas. The argumentation for this choice in given in the Appendix. The stopping power

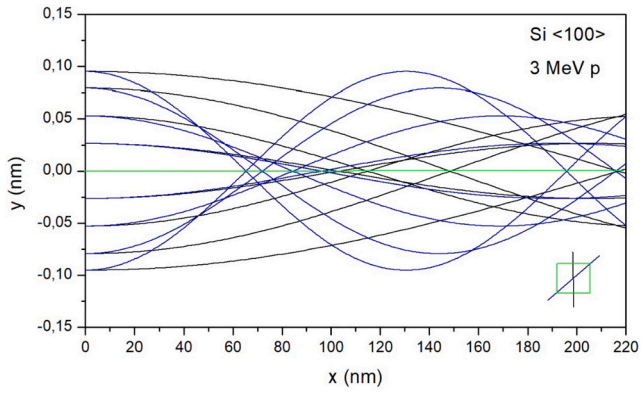

Fig. 6. Proton trajectories in <1 0 0> direction, for two significant oscillation planes.

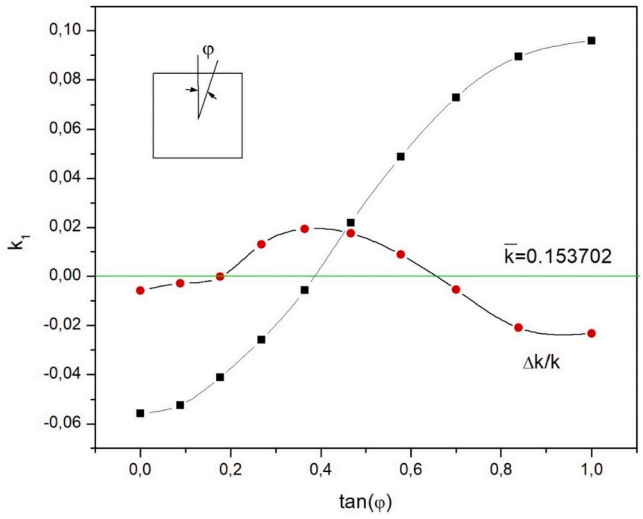

Fig. 7. The coefficient k_1 (in He/a_B4) and variation of the coefficient k (He/a_B^2) from the mean value as a function of tan φ (orientation of the oscillation plane, see insert) for <1 0 0> channel.

essentially depends on the local electron density which was obtained by summing the Hartree-Fock electron densities of neighboring rows; for practical calculation it was approximated by a fitted polynomial. Figs. 5 and 6 show the 3 MeV proton trajectories for <1 1 0> and <1 0 0> orientations, respectively. As we see, virtual focusing appears at first glance better in <1 1 0> channel where the trajectories approach at about 140 nm from the surface. For the <1 0 0> direction, focusing with a diffuse halo appears at about 100 nm from the surface. The energy loss until focusing point for both channels is about 0.64 keV and 0.9 keV, respectively – it is higher for <1 0 0> orientation that has smaller interatomic distances and therefore higher electron density. As shown later, such energy loss is accompanied by scattering straggling that will have a marked influence on the sharpness of the focusing point.

6. Areal distributions

Ray tracing at a much finer distribution can be used to obtain relative particle densities in selected planes perpendicular to the channel axis. The method is similar to Monte Carlo simulations [1–9], however, here we can shoot particles of a uniform areal distribution that allows us to use interpolation procedures in the resulting distribution. The calculation was done for <1 0 0> channel which has a rectangular area, distributing its area into a 100 × 100 mesh. We assumed a circular starting distribution within a circular area of 3.6 a_B diameter, so the

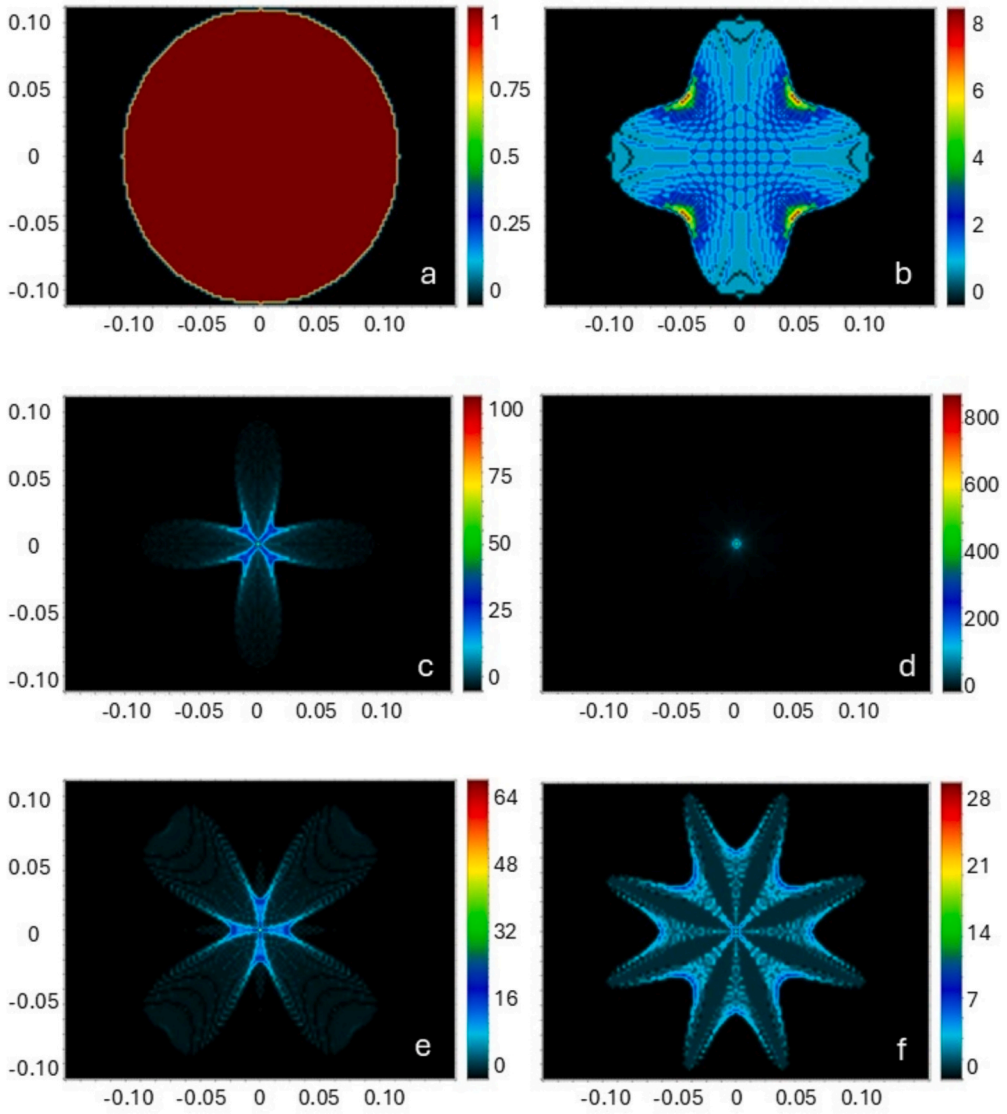

Fig. 8. Relative current density at selected distances along the <1 0 0> channel: 3 nm (a), 40 nm (b), 70 nm (c), 100 nm (d), 140 nm (e), 200 nm (f), omitting the effect of scattering by electrons. Axes in nm. The numerical values of the color scale indicate the gain in current density.

number of initial projectiles was smaller (actual number was 7845). The obtained distributions at selected planes were smoothed by 4-point quadratic interpolation.

For planar distribution, it was necessary to calculate the values of k and k_1 for a general point in the channel cross section area. For a point given as (r, φ) in a polar diagram, the distances to the four neighboring atomic rows are given by the expressions

$$R = \sqrt{\frac{a^2}{2} + r^2 \pm ar(cos\varphi \pm sin\varphi)} \tag{9}$$

with a the unit cell dimension. The dependence of k and k_1 on tan φ is shown in Fig. 7; for practical calculation it was approximated by a polynomial. For calculation of planar distributions, we further assumed that the oscillations remain predominantly planar, gradually becoming helical only deeper in the crystal.

The areal distributions located at 3 nm, 40 nm, 70 nm, 100 nm, 140 nm and 200 nm are shown on Fig. 8. We can see that due to the changing of the sign of k_1 at approximately 21°, the focusing point is quite sharp at 100 nm, with an intensity increase by a factor of 850.

7. Scattering by electrons

Due to multiple scattering by electrons, the projectile trajectories smear, which may alter the ideal picture of Fig. 8. The mean scattering angle was rigorously studied in [18], whose results also reproduce the local density approximation:

$$\delta\theta^2(r) = \frac{4\pi e^4}{m^2 v^4}\rho_e(r)\ln\left(\frac{2m_e v^2}{I}\right) \tag{10}$$

Here e and m_e are electron charge and mass, respectively, ρ_e is electron density, I the average excitation potential and v the projectile velocity. Eq. (10) combined with Bethe-Bloch equation in its simplest form [10], gives

$$\delta\theta^2 = \frac{m_e}{2m}\frac{\Delta E}{E} \tag{11}$$

where ΔE represents energy loss. It should be noted that in SI units, e^2 is replaced by $\alpha\hbar c$, α being the fine structure constant. The factor of ½ in (11) requires some consideration. Equation of the type (11), but without the factor of ½ was first derived by Bohr [19] for multiple scattering of light projectiles (like protons) on target atoms. The author further gives

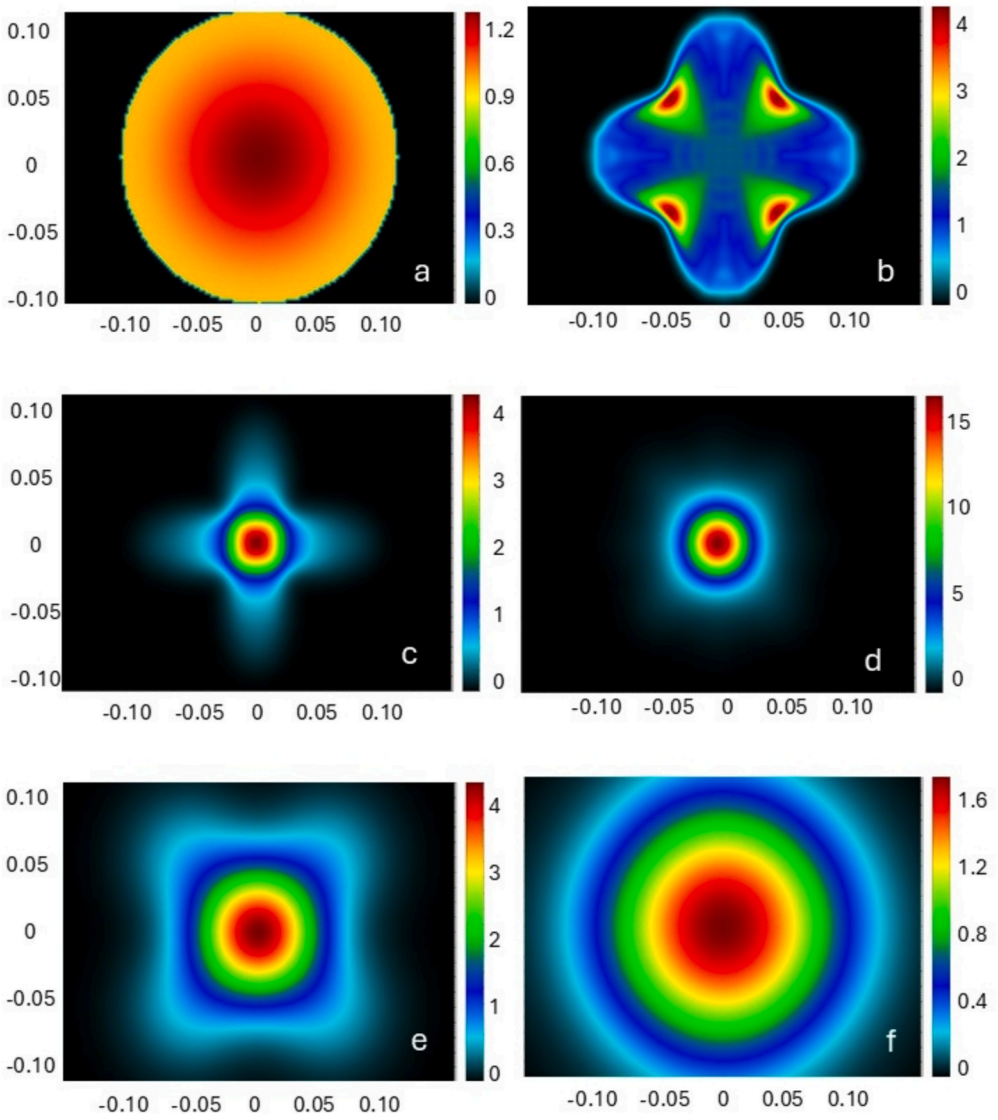

Fig. 9. The same as in Fig. 8 but including the effect on proton scattering by electrons.

a hint that the same equation may also be used for multiple scattering by electrons. The factor of ½ was correctly, but without explanation, included into the expression given by [20]. The mean angular spread of a 3 MeV beam losing about 0.5 keV of its energy is then about 1 min of arc.

A thin parallel beam with a Gaussian distribution $\frac{\exp\left(-\frac{\vartheta^2}{\delta\theta^2}\right)}{\pi\delta\theta^2}$ [19] then smears at the distance z into a diffuse spot whose shape is given by a two-dimensional Gaussian distribution. For straight particle trajectories, its standard deviation would be $\sigma = \delta\theta\ z$, however as the angular spread increases with distance, σ is calculated by the integral

$$\sigma = \int_0^z \delta\theta(x)dx = \frac{2}{3}\delta\theta(z)z \tag{12}$$

here we assumed that for small energy loss, the variation of projectile stopping power with energy can be neglected: $\Delta E = \frac{dE}{dz}z$. For small solid angles $d\Omega = 2\pi\vartheta d\vartheta$, leading to a two-dimensional, axially symmetric planar distribution it further follows $\sigma^2 = 2\ \sigma_x^2 = 2\ \sigma_y^2$.

The influence of electron scattering is shown in Fig. 9 for the same planar distributions at six selected distances. The contribution of each projectile was added to the total yield as a two-dimensional Gaussian distribution. The energy loss and the respective standard deviation were calculated individually for each particle trajectory. As is obviously seen, scattering by electrons almost completely smears out the fine focusing of Fig. 8. At 100 nm, there is still a higher proton density at the central axis of the channel, but this is largely due to smaller energy loss and respective smearing in the middle of the channel. The relative intensity at the channel axis is about 14, which is by a factor of 60 less than on Fig. 8. The second focusing point is almost completely diffused; the smearing may even be larger than calculated, as the projectile motion gradually passes from planar to helical.

Thermal vibrations have little effect on the focusing pattern, at least compared to the effect of electron scattering. Protons of 3 MeV energy pass 100 nm in 4 fs, while the characteristic frequency of optical phonons is of the order 10 GHz. The maximum frequency in the thermal equilibrium ($\hbar\omega = k_B T$) would be 6 THz, which means that the crystals lattice behaves frozen during the proton passage. The focusing pattern is further blurred by the background of particles scattered at large angles that we did not involve in the calculation. Several experimental circumstances may also hinder the focusing effect. Here the most important parameter is collimation of the impact beam that must be kept below 1 min of arc.

8. Scaling relations and comparison with experiments

Fig. 9 demonstrates that the focusing effect of MeV protons is radically reduced due to scattering by electrons. We are now trying to determine a scaling relation of σ^2 which would allow us to find experimental conditions where the focusing effect would be more observable. Starting with eq. (11), the focusing distance is approximately given as a product of projectile velocity and a quarter of oscillation time: $z = v\frac{\pi}{2}\sqrt{\frac{m}{k}}$. Inserting this in eq. (11) rules out the projectile energy in the denominator. Discarding again the energy dependence of the stopping power, we deduce the following relationship:

$$\sigma^2 \approx \frac{\pi^3\sqrt{2}}{18}\frac{m_e}{m\sqrt{k^3}}\frac{dE}{dz}\sqrt{E} \tag{13}$$

As the function $\frac{dE}{dz}\sqrt{E}$ is a decreasing function of energy, Eq. (13) implies that smaller values of σ^2 would be achieved by more massive projectiles and higher energies. The projectile atomic number Z_1 also plays a minor role: the stopping power is approximately proportional to Z_1^2. As the coefficient k is proportional to Z_1 and $m \approx 2Z_1$, σ^2 is then approximately proportional to $1/\sqrt{Z_1}$. For illustration, increasing the proton energy to 60 MeV (by a factor of 20), would reduce σ^2 by a factor of 3 in the focal point. Replacing protons with alphas resulted in a factor of 2.8. Energies in the several 10 MeV range and heavier ions were also used in the calculations of [1–8].

Experimental evidence of the focusing effect was performed by measuring the scattering pattern of particles behind a thin crystal [7–9]. As the scattering angle is given by the ratio of particle transverse and longitudinal velocities, the measured pattern shows the distribution of oscillating velocities, which attains a maximal spread when the particles focus at the exit surface of the crystal. Our calculations confirm that protons indeed focus for the case for 1 MeV protons exiting a crystal of 55 nm thickness [9] and for 7 MeV protons exiting the thickness of 140 nm [7]. The resulting velocity distribution has the shape of the letter X which for 7 MeV protons shows a maximal scattering angle of about 0.09 degrees [7]. Though not our initial aim, we modified our code to see the distribution of scattered particles as well and reproduced the shape of X with the maximal scattering angle of 0.057 degrees. This is somewhat smaller than the experimental value, but it agrees well with the calculated value of about 0.06 degrees of the same authors [7]. In comparison with Monte Carlo values for 1 MeV protons [9], the agreement is also good: 0.17 degrees [9] vs. 0.15 degrees. Regarding the effect of proton scattering by electrons, it is noticeable for 7 MeV protons, but it has a rather strong impact for 1 MeV protons: a rapid increase of the mean scattering angle $\delta\theta$[12] with decreasing proton energy makes the scattering pattern diffuse.

9. Conclusion

An analytical model of amplitude-dependent oscillations perpendicular to the channel axis was developed for transverse movement of channeled particles, which can lead to partial focusing of particles in the near-region below the crystal surface. Dispersion of individual particle trajectories is mainly caused by the anharmonic term of the channel potential. The anharmonic term vanishes at a specific direction in <1 0 0> channel in silicon, allowing for a sharp focusing point with a weak halo. The focusing point is considerably blurred by the dispersion of trajectories on account of multiple scattering by electrons. The intensity of these processes can be reduced by performing experiments with heavier projectiles and energies of several 10 MeV, but in either case, the focusing effect can only be expected for the first (shallowest) focusing point. For further experimentalists, the authors should choose thin crystals of the order of 100 nm that would minimize the scattering effect of crystal electrons and use heavier projectiles with sufficiently high energies, collimated below 1 min of arc.

CRediT authorship contribution statement

Žiga Šmit: Conceptualization, Data curation, Formal analysis, Investigation, Methodology, Software, Writing - original draft, Writing - review & editing. **Esther Punzon-Quijorna:** Visualization, Validation. **Sabina Markelj:** Conceptualization, Writing - review & editing.

Declaration of competing interest

The authors declare that they have no known competing financial interests or personal relationships that could have appeared to influence the work reported in this paper.

Acknowledgements

Two of the authors, Esther Punzon-Quijorna and Sabina Markelj, acknowledge the support from the Slovenian Resarch Agency (research core funding No. P2-0405 and research project No. J2-60052).

Appendix. Stopping power in the channel

Proton stopping in silicon at around 3 MeV is entirely due to scattering by electrons; nuclear stopping contributes 0.06% [21,22]. Stopping of channeling particles is then slower on account of lower electron density. In the MeV energy range, stopping by electrons can be described by a modified Bethe-Bloch equation which contains the electron density as a proportional factor. However, the most critical term in this equation is the logarithmic term as given in (20). Here the excitation potential I represents the lowest possible energy transfer in particle-atom collision and is empirically given as $I \approx Z \times 10$ eV [10]. The channeled particle moves distant from individual atoms and collides with electrons as in a free electron gas. Linhard [17] comprehensively treated interaction of particles with an electron gas and proposed the minimum energy transfer as plasmon excitation with the energy of $\hbar\omega_p$, where ω_p is the plasma frequency

$$\omega_p = \sqrt{\frac{e^2\rho_e}{\varepsilon_0 m_e}} \tag{14}$$

where e and m_e are electron charge and mass, respectively, and ρ_e is electron density. It is noticeable that the stopping power now also depends on electron density through the logarithmic term.

The mean electronic density in silicon can be calculated either from the crystallographic data (considering 8 atoms in the unit cell) or from the density-atomic mass relation; in both cases we get $\rho_e = 6.9917 \times 10^{23}$ cm^{-3}. This density would imply $\hbar\omega_p = 31.05$ eV, which is considerably smaller than the mean atomic potential of approximately 140 eV. Consequently, the calculated stopping power of 298 MeV/cm is 50% higher than the tabulated values of 196.2 MeV/cm of SRIM or PSTAR [21,22]. This value is reproduced by calculation assuming the electron density of 0.63 ρ_e. The reduced density qualitatively suggests that the bound electrons of 1 s and 2 s orbitals (and partly also of 2p) do not contribute to the electron gas:

(14–4)/14 = 0.71. Our HF densities in the center of the <1 0 0> channel show the electron density of 0.285 ρ_e, resulting in the stopping power of 95 MeV/cm. For comparison, dechanneling experiments in silicon [23] show that the mean stopping power in the channel is about 70% of the amorphous value. This implies the electron density to be of about 0.43 ρ_e. The value is sensible as before dechanneling, the particles move in helical orbits closer to the atoms. Based on these values, we then decided to perform calculations with the stopping power of electron gas, using the HF electron densities. A similar approach is used in Monte Carlo calculations [1–4,6] where the electron densities are calculated from the Thomas Fermi potential. We further estimate that the stopping powers may be uncertain by 10%, which will mainly influence the uncertainty in calculating the spread of the projectile trajectories due to collisions with electrons. Since the standard deviation of the scattering angle depends on the square root of the energy loss (11), the stopping power uncertainty will contribute about 5% uncertainty to this value.

References

[1] N. Nešković, Rainbow effect in ion channeling, Phys. Rev. B 33 (1986) 6030–6035.
[2] L. Miletić, S. Petrović, N. Nešković, Decay of zero-degree focusing of channeled ions, Nucl. Instr. Meth. Phys. Res. B 115 (1996) 337–339.
[3] S. Petrović, S. Korica, M. Kokkoris, N. Nešković, Angular distributions of ions channeled in the <100> Si crystals, Nucl. Instr. Meth. Phys. Res. B 193 (2002) 152–159.
[4] N. Starčević, S. Petrović, Universal axial rainbow channeling interaction potential, Eur. Phys. J. D 77 (2023) 61, https://doi.org/10.1140/epjd/s10053-023-00641-5.
[5] Y.N. Demkov, J.D. Meyer, A sub-atomic microscope, superfocusing in channeling and close encounter atomic and nuclear reactions, Eur. Phys. J. B 42 (2004) 361–365, https://doi.org/10.1140/epjb/e2004-00391-6.
[6] S. Petrović, N. Nešković, V. Berec, M. Ćosić, Superfocusing of channeled protons in subatomic measurement resolution, Phys. Rev. A 85 (2012) 032901.
[7] H.F. Krause, S. Datz, P.F. Dittner, J. Gomez del Campo, P.D. Miller, C.D. Moak, N. Nešković, P.L. Pepmiller, Rainbow effect in axial ion channeling, Phys. Rev. B 33 (1986) 6036–6044.
[8] H.F. Krause, J.H. Barrett, S. Datz, P.F. Dittner, N.L. Jones, J. Gomez del Campo, C. R. Vane, Angular distribution of ions axially channeled in a very thin crystal: Experimental and theoretical results, Phys. Rev. A 49 (1994) 283–299.
[9] M. Motapothula, S. Petrović, N. Nešković, M.B.H. Breese, Experimental evidence of the superfocusing effect for axially channeled MeV protons, Phys. Rev. B 94 (2016), https://doi.org/10.1103/PhysRevB.94.075415.
[10] J. Lindhard, Influence of crystal lattice on the motion of energetic charged particles, Mat. Fys. Medd. Dan. Vid. Selsk. 34 (14) (1965).
[11] C. Froese Fisher, General Hartree-Fock program, Comp. Phys. Comm. 43 (1987) 355–365, https://doi.org/10.1016/0010-4655(87)90053-1.
[12] L.D. Landau, E.M. Lifshitz, Quantum Mechanics (Non-Relativistic Theory), Pergamon Press, Oxford, 1977, pp. 259–264.
[13] F.M. Fernández, Comment on: "Series solution to the Thomas–Fermi equation" [Phys. Lett. A 365 (2007) 111], Phys. Lett. A 372 (2008) 5258–5260.
[14] G. Molière, Theorie der Streuung schneller geladener Teilchen I Einzelstreuung am abgeschirmten Coulomb-Feld, Z. Naturforschg. 2a (1947) 133–145.
[15] D. Davis, Thomas-Fermi screening in one dimension, Phys. Rev. B 7 (1973) 129–135.
[16] S.C. Brenner, L.R. Scott, The Mathematical Theory of Finite Element Methods, 3rd ed., Springer, 2008, pp. 1–4.
[17] J. Lindhard, On the properties of a gas of charged particles, Mat. Fys. Medd. Dan. Vid. Selsk. 28 (8) (1954).
[18] V.A. Ryabov, The angular spread of fast ions scattered by atomic electrons, Phys. Lett. A 153 (1991) 251–256.
[19] N. Bohr, The penetration of atomic particles through matter, Mat. Fys. Medd. Dan. Vid. Selsk. 18 (8) (1948).
[20] D.S. Gemmell, Channelling and related effects in the motion of charged particles through crystals, Rev. Mod. Phys. Rev. Mod. Phys. 46 (1) (1974) 129–227.
[21] www.srim.org.
[22] physics.nist.gov/PhysRefData/Star/Text/PSTAR.html.
[23] S. Shafiei, M. Lamehi-Rachti, The study of channeling parameters of protons along axial and planar directions of Si, Nucl. Instr. Meth. Phys. Res. B 515 (2022) 7–13.